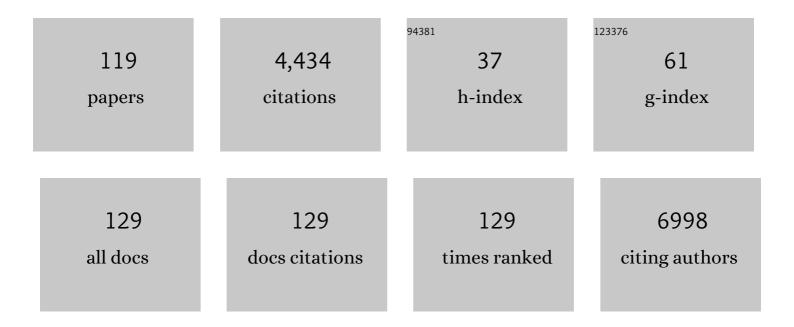
Louise van der Weerd

List of Publications by Year in descending order

Source: https://exaly.com/author-pdf/5266107/publications.pdf Version: 2024-02-01



#	Article	IF	CITATIONS
1	Histopathological correlates of haemorrhagic lesions on <i>ex vivo</i> magnetic resonance imaging in immunized Alzheimer's disease cases. Brain Communications, 2022, 4, fcac021.	1.5	7
2	Co-expression patterns of microglia markers Iba1, TMEM119 and P2RY12 in Alzheimer's disease. Neurobiology of Disease, 2022, 167, 105684.	2.1	45
3	Corpus callosum lesions are associated with worse cognitive performance in cerebral amyloid angiopathy. Brain Communications, 2022, 4, .	1.5	7
4	lron accumulation induces oxidative stress, while depressing inflammatory polarization in human iPSC-derived microglia. Stem Cell Reports, 2022, 17, 1351-1365.	2.3	25
5	Quantitative susceptibility mapping in the thalamus and basal ganglia of systemic lupus erythematosus patients with neuropsychiatric complaints. NeuroImage: Clinical, 2021, 30, 102637.	1.4	2
6	Effects of Long-Term Endogenous Corticosteroid Exposure on Brain Volume and Glial Cells in the AdKO Mouse. Frontiers in Neuroscience, 2021, 15, 604103.	1.4	24
7	Cerebral blood flow and cerebrovascular reactivity are preserved in a mouse model of cerebral microvascular amyloidosis. ELife, 2021, 10, .	2.8	12
8	Iron loading is a prominent feature of activated microglia in Alzheimer's disease patients. Acta Neuropathologica Communications, 2021, 9, 27.	2.4	79
9	Vascular Hypothesis of Alzheimer Disease. Arteriosclerosis, Thrombosis, and Vascular Biology, 2021, 41, 1265-1283.	1.1	37
10	Occipital Cortical Calcifications in Cerebral Amyloid Angiopathy. Stroke, 2021, 52, 1851-1855.	1.0	2
11	Quantification of different iron forms in the aceruloplasminemia brain to explore iron-related neurodegeneration. NeuroImage: Clinical, 2021, 30, 102657.	1.4	8
12	Offâ€resonance saturation as an MRI method to quantify mineral―iron in the postâ€mortem brain. Magnetic Resonance in Medicine, 2021, , .	1.9	4
13	MR imaging for the quantitative assessment of brain iron in aceruloplasminemia: A postmortem validation study. Neurolmage, 2021, 245, 118752.	2.1	3
14	Expandable human cardiovascular progenitors from stem cells for regenerating mouse heart after myocardial infarction. Cardiovascular Research, 2020, 116, 545-553.	1.8	10
15	Progression and Classification of Granular Osmiophilic Material (GOM) Deposits in Functionally Characterized Human NOTCH3 Transgenic Mice. Translational Stroke Research, 2020, 11, 517-527.	2.3	16
16	Effects of Alzheimer's disease and formalin fixation on the different mineralised-iron forms in the human brain. Scientific Reports, 2020, 10, 16440.	1.6	17
17	Pathological characterization of T2*-weighted MRI contrast in the striatum of Huntington's disease patients. NeuroImage: Clinical, 2020, 28, 102498.	1.4	9
18	CSF enhancement on post-contrast fluid-attenuated inversion recovery images; a systematic review. NeuroImage: Clinical, 2020, 28, 102456.	1.4	12

LOUISE VAN DER WEERD

#	Article	IF	CITATIONS
19	The coarse-grained plaque: a divergent Aβ plaque-type in early-onset Alzheimer's disease. Acta Neuropathologica, 2020, 140, 811-830.	3.9	45
20	A novel type of amyloidâ€beta plaques identified in earlyâ€onset AD. Alzheimer's and Dementia, 2020, 16, e040626.	0.4	0
21	Strategic corpus callosum lesions are associated with worse cognitive performance in cerebral amyloid angiopathy. Alzheimer's and Dementia, 2020, 16, e042464.	0.4	0
22	Cerebral amyloid angiopathy-linked β-amyloid mutations promote cerebral fibrin deposits via increased binding affinity for fibrinogen. Proceedings of the National Academy of Sciences of the United States of America, 2020, 117, 14482-14492.	3.3	24
23	Quantitative MRI and laser ablation-inductively coupled plasma-mass spectrometry imaging of iron in the frontal cortex of healthy controls and Alzheimer's disease patients. NeuroImage, 2020, 215, 116808.	2.1	21
24	Amyloid imaging of dutchâ€ŧype hereditary cerebral amyloid angiopathy carriers. Annals of Neurology, 2019, 86, 616-625.	2.8	22
25	Influence of different isoflurane anesthesia protocols on murine cerebral hemodynamics measured with pseudoâ€continuous arterial spin labeling. NMR in Biomedicine, 2019, 32, e4105.	1.6	29
26	Normal Aging Brain Collection Amsterdam (NABCA): A comprehensive collection of postmortem high-field imaging, neuropathological and morphometric datasets of non-neurological controls. NeuroImage: Clinical, 2019, 22, 101698.	1.4	25
27	Osteopontin and phospho‧MAD2/3 are associated with calcification of vessels in D AA, an hereditary cerebral amyloid angiopathy. Brain Pathology, 2019, 29, 793-802.	2.1	15
28	Imaging beta amyloid aggregation and iron accumulation in Alzheimer's disease using quantitative susceptibility mapping MRI. NeuroImage, 2019, 191, 176-185.	2.1	122
29	7T MRI allows detection of disturbed cortical lamination of the medial temporal lobe in patients with Alzheimer's disease. NeuroImage: Clinical, 2019, 21, 101665.	1.4	28
30	Multicenter reproducibility of quantitative susceptibility mapping in a gadolinium phantom using MEDI+0 automatic zero referencing. Magnetic Resonance in Medicine, 2019, 81, 1229-1236.	1.9	31
31	Quantitative comparison of different iron forms in the temporal cortex of Alzheimer patients and control subjects. Scientific Reports, 2018, 8, 6898.	1.6	40
32	TGFβ pathway deregulation and abnormal phospho‧MAD2/3 staining in hereditary cerebral hemorrhage with amyloidosisâ€Dutch type. Brain Pathology, 2018, 28, 495-506.	2.1	15
33	Postmortem MRI and histology demonstrate differential iron accumulation and cortical myelin organization in early- and late-onset Alzheimer's disease. Neurobiology of Aging, 2018, 62, 231-242.	1.5	93
34	9.4T and 17.6T MRI of Retinoblastoma: Ex Vivo evaluation of microstructural anatomy and disease extent compared with histopathology. Journal of Magnetic Resonance Imaging, 2018, 47, 1487-1497.	1.9	7
35	Transit time mapping in the mouse brain using timeâ€encoded pCASL. NMR in Biomedicine, 2018, 31, e3855.	1.6	28
36	P3â€450: COARSE PLAQUES ARE MORE COMMON IN EARLY ONSET COMPARED TO LATE ONSET ALZHEIMER'S DISEASE. Alzheimer's and Dementia, 2018, 14, P1290.	0.4	0

#	Article	IF	CITATIONS
37	ICâ€Pâ€122: THE NORMAL AGING BRAIN COLLECTION AMSTERDAM (NABCA): A COMPREHENSIVE COLLECTION (POSTMORTEM IMAGING, NEUROPATHOLOGICAL AND MORPHOMETRIC DATASETS. Alzheimer's and Dementia, 2018, 14, P103.	OF 0.4	0
38	P2â€274: MAPPING OF NATRIURETIC PEPTIDES AND THEIR RECEPTORS IN THE BRAINS OF NONâ€DEMENTED HUMAN SUBJECTS AND PATIENTS WITH ALZHEIMER'S DISEASE. Alzheimer's and Dementia, 2018, 14, P782.	0.4	0
39	Natriuretic Peptides in Post-mortem Brain Tissue and Cerebrospinal Fluid of Non-demented Humans and Alzheimer's Disease Patients. Frontiers in Neuroscience, 2018, 12, 864.	1.4	13
40	P2â€477: THE NORMAL AGING BRAIN COLLECTION AMSTERDAM (NABCA): A COMPREHENSIVE COLLECTION OF POSTMORTEM IMAGING, NEUROPATHOLOGICAL AND MORPHOMETRIC DATASETS. Alzheimer's and Dementia, 2018, 14, P907.	0.4	0
41	Cerebral Amyloid Angiopathy With Vascular Iron Accumulation and Calcification. Stroke, 2018, 49, 2081-2087.	1.0	15
42	Voluntary exercise improves muscle function and does not exacerbate muscle and heart pathology in aged Duchenne muscular dystrophy mice. Journal of Molecular and Cellular Cardiology, 2018, 125, 29-38.	0.9	15
43	Postmortem T2*- Weighted MRI Imaging of Cortical Iron Reflects Severity of Alzheimer's Disease. Journal of Alzheimer's Disease, 2018, 65, 1125-1137.	1.2	47
44	Brain Transcriptomic Analysis of Hereditary Cerebral Hemorrhage With Amyloidosis-Dutch Type. Frontiers in Aging Neuroscience, 2018, 10, 102.	1.7	13
45	Influence of full-length dystrophin on brain volumes in mouse models of Duchenne muscular dystrophy. PLoS ONE, 2018, 13, e0194636.	1.1	10
46	Experimental Models of Brain Disease: MRI Contrast Mechanisms for the Assessment of Pathophysiological Status. , 2018, , 63-92.		0
47	The Evolution of Fangs, Venom, and Mimicry Systems in Blenny Fishes. Current Biology, 2017, 27, 1184-1191.	1.8	36
48	Continuous infusion of manganese improves contrast and reduces side effects in manganese-enhanced magnetic resonance imaging studies. NeuroImage, 2017, 147, 1-9.	2.1	20
49	Endless forms most beautiful: the evolution of ophidian oral glands, including the venom system, and the use of appropriate terminology for homologous structures. Zoomorphology, 2017, 136, 107-130.	0.4	38
50	Human-brain ferritin studied by muon spin rotation: a pilot study. Journal of Physics Condensed Matter, 2017, 29, 415801.	0.7	13
51	[O1–08–04]: IRON AND MYELIN AS SOURCES OF MRI CONTRAST IN PATIENTS WITH ALZHEIMER'S DISEASE. Alzheimer's and Dementia, 2017, 13, P208.	0.4	Ο
52	Cortical Iron Reflects Severity ofÂAlzheimer's Disease. Journal of Alzheimer's Disease, 2017, 60, 1533-1545.	1.2	119
53	A novel approach to quantify different iron forms in ex-vivo human brain tissue. Scientific Reports, 2016, 6, 38916.	1.6	33
54	Bis-pyridylethenyl benzene as novel backbone for amyloid-β binding compounds. Bioorganic and Medicinal Chemistry, 2016, 24, 6139-6148.	1.4	5

#	Article	IF	CITATIONS
55	The NOTCH3 score: a pre-clinical CADASIL biomarker in a novel human genomic NOTCH3 transgenic mouse model with early progressive vascular NOTCH3 accumulation. Acta Neuropathologica Communications, 2015, 3, 89.	2.4	20
56	Camelid heavy chain only antibody fragment domain against βâ€site of amyloid precursor protein cleaving enzyme 1 inhibits βâ€secretase activity <i>inĂvitro</i> and <i>inÂvivo</i> . FEBS Journal, 2015, 282, 3618-3631.	2.2	15
57	Enhanced glutathione PEGylated liposomal brain delivery of an anti-amyloid single domain antibody fragment in a mouse model for Alzheimer's disease. Journal of Controlled Release, 2015, 203, 40-50.	4.8	114
58	Fusion of hIgG1-Fc to 111In-anti-amyloid single domain antibody fragment VHH-pa2H prolongs blood residential time in APP/PS1 mice but does not increase brain uptake. Nuclear Medicine and Biology, 2015, 42, 695-702.	0.3	47
59	Potential role of antimicrobial peptides in the early onset of Alzheimer's disease. Alzheimer's and Dementia, 2015, 11, 51-57.	0.4	58
60	Scattered Deletion of PKD1 in Kidneys Causes a Cystic Snowball Effect and Recapitulates Polycystic Kidney Disease. Journal of the American Society of Nephrology: JASN, 2015, 26, 1322-1333.	3.0	60
61	In vivo bioluminescence imaging of vascular remodeling after stroke. Frontiers in Cellular Neuroscience, 2014, 8, 274.	1.8	29
62	Threeâ€dimensional inversion recovery manganeseâ€enhanced MRI of mouse brain using superâ€resolution reconstruction to visualize nuclei involved in higher brain function. NMR in Biomedicine, 2014, 27, 749-759.	1.6	2
63	Polyfluorinated bis-styrylbenzenes as amyloid-β plaque binding ligands. Bioorganic and Medicinal Chemistry, 2014, 22, 2469-2481.	1.4	16
64	Low dystrophin levels in heart can delay heart failure in mdx mice. Journal of Molecular and Cellular Cardiology, 2014, 69, 17-23.	0.9	47
65	Interactive Local Super-Resolution Reconstruction of Whole-Body MRI Mouse Data: A Pilot Study with Applications to Bone and Kidney Metastases. PLoS ONE, 2014, 9, e108730.	1.1	3
66	Mouse Models to Study the Effect of Cardiovascular Risk Factors on Brain Structure and Cognition. Journal of Cerebral Blood Flow and Metabolism, 2013, 33, 1666-1684.	2.4	78
67	Contrast enhancement by lipidâ€based MRI contrast agents in mouse atherosclerotic plaques; a longitudinal study. Contrast Media and Molecular Imaging, 2013, 8, 63-71.	0.4	7
68	Low dystrophin levels increase survival and improve muscle pathology and function in dystrophin/utrophin doubleâ€knockout mice. FASEB Journal, 2013, 27, 2484-2495.	0.2	94
69	Cardiac Dysfunction in Pneumovirus-Induced Lung Injury in Mice. Pediatric Critical Care Medicine, 2013, 14, e243-e249.	0.2	5
70	Squeezers and Leaf-cutters: Differential Diversification and Degeneration of the Venom System in Toxicoferan Reptiles. Molecular and Cellular Proteomics, 2013, 12, 1881-1899.	2.5	52
71	Scavenger Receptor-Al–Targeted Iron Oxide Nanoparticles for In Vivo MRI Detection of Atherosclerotic Lesions. Arteriosclerosis, Thrombosis, and Vascular Biology, 2013, 33, 1812-1819.	1.1	59
72	Molecular Magnetic Resonance Imaging for the Detection of Vulnerable Plaques. Arteriosclerosis, Thrombosis, and Vascular Biology, 2013, , .	1.1	0

#	Article	IF	CITATIONS
73	MR Microscopy of Human Amyloid-β Deposits: Characterization of Parenchymal Amyloid, Diffuse Plaques, and Vascular Amyloid. Journal of Alzheimer's Disease, 2013, 34, 1037-1049.	1.2	17
74	Self-Gated CINE MRI for Combined Contrast-Enhanced Imaging and Wall-Stiffness Measurements of Murine Aortic Atherosclerotic Lesions. PLoS ONE, 2013, 8, e57299.	1.1	4
75	Super-resolution in MRI: better images faster?. Proceedings of SPIE, 2012, , .	0.8	4
76	Histological validation of iron-oxide and gadolinium based MRI contrast agents in experimental atherosclerosis: The do's and don't's. Atherosclerosis, 2012, 225, 274-280.	0.4	11
77	Assessment of cardiac function in three mouse dystrophinopathies by magnetic resonance imaging. Neuromuscular Disorders, 2012, 22, 418-426.	0.3	19
78	P4â€001: Overactivation of NMDA receptors in the aged APPsweâ€₽S1dE9 brain, a mouse model of Alzheimer's disease. Alzheimer's and Dementia, 2012, 8, P638.	0.4	0
79	Superâ€resolution methods in MRI: Can they improve the tradeâ€off between resolution, signalâ€toâ€noise ratio, and acquisition time?. Magnetic Resonance in Medicine, 2012, 68, 1983-1993.	1.9	187
80	In Vivo Detection of Amyloid-β Deposits Using Heavy Chain Antibody Fragments in a Transgenic Mouse Model for Alzheimer's Disease. PLoS ONE, 2012, 7, e38284.	1.1	34
81	Highâ€field MRI of single histological slices using an inductively coupled, selfâ€resonant microcoil: application to <i>ex vivo</i> samples of patients with Alzheimer's disease. NMR in Biomedicine, 2011, 24, 351-357.	1.6	36
82	Pre-clinical optical imaging and MRI for drug development in Alzheimer's disease. Drug Discovery Today: Technologies, 2011, 8, e117-e125.	4.0	8
83	Initial stress in biomechanical models of atherosclerotic plaques. Journal of Biomechanics, 2011, 44, 2376-2382.	0.9	46
84	Pretreatment with Interferon-Î ³ Enhances the Therapeutic Activity of Mesenchymal Stromal Cells in Animal Models of Colitis. Stem Cells, 2011, 29, 1549-1558.	1.4	287
85	MRI artifacts in human brain tissue after prolonged formalin storage. Magnetic Resonance in Medicine, 2011, 65, 1750-1758.	1.9	47
86	In vivo biodistribution of stem cells using molecular nuclear medicine imaging. Journal of Cellular Physiology, 2011, 226, 1444-1452.	2.0	41
87	MRI in Animal Models of Psychiatric Disorders. Methods in Molecular Biology, 2011, 771, 309-335.	0.4	3
88	Volumetry and Other Quantitative Measurements to Assess the Rodent Brain. Methods in Molecular Biology, 2011, 771, 277-291.	0.4	0
89	The time window of MRI of murine atherosclerotic plaques after administration of CB2 receptor targeted micelles: interâ€scan variability and relation between plaque signal intensity increase and gadolinium content of inversion recovery prepared versus nonâ€prepared fast spin echo. NMR in Biomedicine. 2010. 23. 939-951.	1.6	5
90	Cell tracking using iron oxide fails to distinguish dead from living transplanted cells in the infarcted heart. Magnetic Resonance in Medicine, 2010, 63, 817-821.	1.9	45

LOUISE VAN DER WEERD

#	Article	IF	CITATIONS
91	Overexpression of Heat Shock Protein 27 Reduces Cortical Damage after Cerebral Ischemia. Journal of Cerebral Blood Flow and Metabolism, 2010, 30, 849-856.	2.4	45
92	Functional and Structural Diversification of the Anguimorpha Lizard Venom System. Molecular and Cellular Proteomics, 2010, 9, 2369-2390.	2.5	70
93	MRâ^'Based Molecular Imaging of the Brain: The Next Frontier. American Journal of Neuroradiology, 2010, 31, 1577-1583.	1.2	12
94	Cerebral Amyloidosis: Postmortem Detection with Human 7.0-T MR Imaging System. Radiology, 2009, 253, 788-796.	3.6	49
95	The 3D Moore-Rayleigh Test for the Quantitative Groupwise Comparison of MR Brain Images. Lecture Notes in Computer Science, 2009, 21, 564-575.	1.0	3
96	Nonâ€invasive tracking of avian development <i>in vivo</i> by MRI. NMR in Biomedicine, 2009, 22, 365-373.	1.6	27
97	Changes in GABA _A receptor properties in amygdala kindled animals: In vivo studies using [¹¹ C]flumazenil and positron emission tomography. Epilepsia, 2009, 50, 88-98.	2.6	43
98	Evolution and diversification of the Toxicofera reptile venom system. Journal of Proteomics, 2009, 72, 127-136.	1.2	91
99	A central role for venom in predation by <i>Varanus komodoensis</i> (Komodo Dragon) and the extinct giant <i>Varanus</i> (<i>Megalania</i>) <i>priscus</i> . Proceedings of the National Academy of Sciences of the United States of America, 2009, 106, 8969-8974.	3.3	120
100	Evolution of an Arsenal. Molecular and Cellular Proteomics, 2008, 7, 215-246.	2.5	298
101	Automated segmentation of the ex vivo mouse brain. , 2007, , .		2
102	Cognitive deficits in <i>Tsc1</i> ^{+/â^'} mice in the absence of cerebral lesions and seizures. Annals of Neurology, 2007, 62, 648-655.	2.8	233
103	<i>T</i> ₁ relaxation in in vivo mouse brain at ultraâ€high field. Magnetic Resonance in Medicine, 2007, 58, 390-395.	1.9	32
104	Regional Variation of Cerebral Blood Flow and Arterial Transit Time in the Normal and Hypoperfused Rat Brain Measured Using Continuous Arterial Spin Labeling MRI. Journal of Cerebral Blood Flow and Metabolism, 2006, 26, 274-282.	2.4	50
105	Neuroprotective Effects of Virally Delivered HSPs in Experimental Stroke. Journal of Cerebral Blood Flow and Metabolism, 2006, 26, 371-381.	2.4	60
106	The Chronic Vascular and Haemodynamic Response after Permanent Bilateral Common Carotid Occlusion in Newborn and Adult Rats. Journal of Cerebral Blood Flow and Metabolism, 2006, 26, 1066-1075.	2.4	108
107	Gradual changes in the apparent diffusion coefficient of water in selectively vulnerable brain regions following brief ischemia in the gerbil. Magnetic Resonance in Medicine, 2005, 53, 593-600.	1.9	6
108	Neuroprotective effects of HSP70 overexpression after cerebral ischaemia—An MRI study. Experimental Neurology, 2005, 195, 257-266.	2.0	56

LOUISE VAN DER WEERD

#	Article	IF	CITATIONS
109	Heat shock protein overexpression - effect on experimental stroke. Journal of Cerebral Blood Flow and Metabolism, 2005, 25, S508-S508.	2.4	0
110	A comparison of FAIR and CASL perfusion imaging in mice. Journal of Cerebral Blood Flow and Metabolism, 2005, 25, S343-S343.	2.4	0
111	Vascular and haemodynamic response following chronic hypoperfusion in the developing and mature rat. Journal of Cerebral Blood Flow and Metabolism, 2005, 25, S218-S218.	2.4	0
112	MRI of Animal Models of Brain Disease. Methods in Enzymology, 2004, 386, 149-177.	0.4	11
113	MR image-guided investigation of regional signal transducers and activators of transcription-1 activation in a rat model of focal cerebral ischemia. Neuroscience, 2004, 127, 333-339.	1.1	23
114	Modelling of Self-diffusion and Relaxation Time NMR in Multicompartment Systems with Cylindrical Geometry. Journal of Magnetic Resonance, 2002, 156, 213-221.	1.2	46
115	Water-conducting properties of lipids during pollen hydration. Plant, Cell and Environment, 2002, 25, 513-519.	2.8	43
116	Nuclear magnetic resonanceimaging of membrane permeability changes in plants during osmoticstress. Plant, Cell and Environment, 2002, 25, 1539-1549.	2.8	64
117	Quantitative NMR microscopy of osmotic stress responses in maize and pearl millet. Journal of Experimental Botany, 2001, 52, 2333-2343.	2.4	76
118	Evaluation of algorithms for analysis of NMR relaxation decay curves. Magnetic Resonance Imaging, 2000, 18, 1151-1158.	1.0	37
119	Orientation of the Phylloquinone Electron Acceptor Anion Radical in Photosystem I. Biochemistry, 1997. 36, 9297-9303.	1.2	78